American Mineralogist, Volume 90, pages 199–205, 2005

A synchrotron Mössbauer spectroscopy study of $(Mg,Fe)SiO_3$ perovskite up to 120 GPa

JENNIFER M. JACKSON,[1,*] WOLFGANG STURHAHN,[2] GUOYIN SHEN,[3] JIYONG ZHAO,[2] MICHAEL Y. HU,[4,5] DANIEL ERRANDONEA,[4,5,†] JAY D. BASS,[1] AND YINGWEI FEI[5]

[1]Department of Geology, University of Illinois at Urbana-Champaign, Illinois 61801, U.S.A.
[2]Advanced Photon Source, Argonne National Laboratory, Illinois 60439, U.S.A.
[3]Consortium for Advanced Radiation Sources, University of Chicago, Illinois 60637, U.S.A.
[4]HP-CAT, Advanced Photon Source, Argonne National Laboratory, Illinois 60439, U.S.A.
[5]Carnegie Institution of Washington, 5251 Broad Branch Road, N.W., Washington, D.C. 20015, U.S.A.

ABSTRACT

The electronic environment of the Fe nuclei in two silicate perovskite samples, $Fe_{0.05}Mg_{0.95}SiO_3$ (Pv05) and $Fe_{0.1}Mg_{0.9}SiO_3$ (Pv10), have been measured to 120 GPa and 75 GPa, respectively, at room temperature using diamond anvil cells and synchrotron Mössbauer spectroscopy (SMS). Such investigations of extremely small and dilute ^{57}Fe-bearing samples have become possible through the development of SMS. Our results are explained in the framework of the "three-doublet" model, which assumes two Fe^{2+}-like sites and one Fe^{3+}-like site that are well distinguishable by the hyperfine fields at the location of the Fe nuclei. At low pressures, $Fe^{3+}/\Sigma Fe$ is about 0.40 for both samples. Our results show that at pressures extending into the lowermost mantle the fraction of Fe^{3+} remains essentially unchanged, indicating that pressure alone does not alter the valence states of iron in $(Mg,Fe)SiO_3$ perovskite. The quadrupole splittings of all Fe sites first increase with increasing pressure, which suggests an increasingly distorted (noncubic) local iron environment. Above pressures of 40 GPa for Pv10 and 80 GPa for Pv05, the quadrupole splittings are relatively constant, suggesting an increasing resistance of the lattice against further distortion. Around 70 GPa, a change in the volume dependence of the isomer shift could be indicative of the endpoint of a continuous transition of Fe^{3+} from a high-spin to a low-spin state.

INTRODUCTION

Iron-bearing magnesium silicate perovskite, coexisting with small amounts of (Mg,Fe)O ferropericlase and $CaSiO_3$ perovskite, is thought to be the most abundant phase in Earth's lower mantle (e.g., Liu 1974; Jeanloz and Thompson 1983; Anderson and Bass 1986; Ito 1989; Fiquet et al. 2000; Weidner and Wang 2000). Knowledge of the physical and chemical properties of such phases under conditions approaching those of the lower mantle is therefore essential to our understanding of the deep mantle. Of particular importance is the electronic state of iron-bearing magnesium silicate perovskite, because it can affect electrostatic charge balance and equilibrium defect concentrations. Properties highly sensitive to such effects include rheology, transport properties, solubility of volatiles, and partitioning of major and trace elements in the lower mantle (e.g., McCammon 1998a). For example, the electrical conductivity of lower mantle phases is strongly influenced by the valence state of iron (Li and Jeanloz 1990; Li et al. 1993; Xu et al. 1998; Katsura et al. 1998). X-ray emission spectroscopic (XES) data recently demonstrated a pressure-induced gradual loss of magnetic moment of the iron component in iron-bearing $MgSiO_3$ perovskite (Li et al. 2003). Experiments on lower mantle phases suggest that iron-bearing magnesium silicate perovskite is the principal sink for ferric iron in the Earth's lower mantle (McCammon 1997, 1998a; McCammon et al. 1998). Therefore, knowledge of the behavior of iron in perovskite under the pressure conditions of the lower mantle is necessary for our understanding of this region within the Earth.

There have been numerous studies performed on the crystal chemistry of $(Mg,Fe)SiO_3$ perovskite, including extended X-ray absorption fine structure (EXAFS) (Jackson et al. 1987; Farges et al. 1994), optical absorption spectroscopy (Shen et al. 1994; Keppler et al. 1994), single-crystal X-ray diffraction (e.g., Kudoh et al. 1990; Ross and Hazen 1990), electron microscopy (Wang et al. 1992), high-resolution powder X-ray diffraction (e.g., Parise et al. 1990; Mao et al. 1991; Jephcoat et al. 1999), atomistic simulations (Richmond and Brodholt 1998), XES (Li et al. 2003), and ^{57}Fe Mössbauer spectroscopy (MBS) under ambient conditions (e.g., Jeanloz et al. 1992; Lauterbach et al. 2000) and at a range of temperatures (McCammon et al. 1992; Fei et al. 1994; McCammon 1998b). Nevertheless, in situ measurements of the pressure dependence of the proportion of Fe^{2+} and Fe^{3+} in $(Mg,Fe)SiO_3$ perovskite have not been performed.

Direct information on the electronic behavior of iron can be obtained by using Mössbauer spectroscopy. Conventional Mössbauer spectroscopy has been performed up to Mbar pressures in a diamond anvil cell using iron-concentrated samples (Pasternak et al. 1997). However, experiments under very high pressure using small samples (<50 μm) containing dilute iron concentrations (≤10 mol% iron) have not been performed with conventional

* E-mail: jmjackso@uiuc.edu
† Current address: Department of Applied Physics, University of Valencia, E-46100 Burjassot, Spain

Mössbauer spectroscopy, because the signals are too low. Recent developments in synchrotron Mössbauer spectroscopy (SMS) have led to an increase in photon flux density by many orders of magnitude (Gerdau and Waard 1999/2000; Sturhahn 2004). Agreement between SMS and MBS has been explicitly demonstrated with powdered samples (e.g., Alp et al. 1995). SMS was used to characterize heterogeneous electron-transfer kinetics, and analysis of reaction end-member specimens by both SMS and MBS yielded comparable Mössbauer parameters, such as Fe^{2+}/Fe^{3+} area ratios (Amonette et al. 2003). SMS was also used to monitor the electronic state of Fe^{2+} in hedenbergite ($CaFeSi_2O_6$) at pressures up to 68 GPa in a diamond anvil cell (Zhang et al. 1999). The goal of this study is to observe the quadrupole splitting and weight fraction at the sites of the ^{57}Fe nuclei to monitor the valence states of iron in (Mg,Fe)SiO_3 perovskite under the pressure conditions where it is considered to be stable in the Earth's interior. In the present study, we extended the sensitivity limits of SMS and measured the electronic state of iron in (Mg,Fe)SiO_3 perovskite between ambient pressure and 120 GPa using diamond anvil cells.

Experimental method

Sample description

The (Mg,Fe)SiO_3 perovskite samples used in the present study are from the same synthesis experiment charge as described in Fei et al. (1994). Briefly, the starting materials were synthetic $Fe_{0.05}Mg_{0.95}SiO_3$ and $Fe_{0.1}Mg_{0.9}SiO_3$ orthopyroxenes (92% ^{57}Fe-enriched). The two perovskite samples were synthesized in a rhenium capsule using the multi-anvil apparatus at The State University of New York (Stony Brook) at 26 GPa and 1873 K for $^{57}Fe_{0.05}Mg_{0.95}SiO_3$ (Pv05) and 1923 K for $^{57}Fe_{0.1}Mg_{0.9}SiO_3$ (Pv10). Both perovskite samples were examined optically, with a powder X-ray diffractometer, and with an electron microprobe, giving the following bulk compositions: $Mg_{0.951(7)}Fe_{0.050(5)}Si_{0.999(4)}O_3$ and $Mg_{0.906(10)}Fe_{0.097(5)}Si_{0.997(5)}O_3$ (Fei et al. 1994). Details of the iron site occupancy in perovskite will be discussed later. Trace amounts of stishovite were present in the diffraction spectra, but the concentration of iron in stishovite is negligible at these compositions (Kesson et al. 1995; Hirose et al. 1999; Miyajima et al. 1999). More details of the sample synthesis and characterization can be found in Fei et al. (1994).

SMS method

We investigated the perovskite samples (Pv05 and Pv10) using the recently developed technique of synchrotron Mössbauer spectroscopy (SMS). Similar to conventional Mössbauer spectroscopy (MBS) this method permits us to determine distortions of electronic charges at the position of the ^{57}Fe nuclei. The configuration of the electron shell and the deviation of the local environment from cubic symmetry expresses itself in two parameters that are accessible to SMS measurements, the splitting of the excited nuclear state caused by an electric-field-gradient tensor (quadrupole splitting) and a shift of the nuclear states caused by the s-electron density in the nuclear volume (isomer shift). Other parameters like magnetic fields can also be routinely obtained but are of no relevance in the present case.

The basic principles of SMS have been described previously (Sturhahn et al. 1998; Gerdau and Waard 1999/2000; Sturhahn 2004), and the advantages of synchrotron-based techniques for high-pressure research using diamond anvil cells (DAC) have been recognized in general (e.g., Hemley 1998) and for SMS in particular (e.g., Zhang et al. 1999; Lübbers et al. 1999). The different experimental approaches of more traditional methods of MBS (e.g., Hawthorne 1988) and SMS are illustrated in Figure 1, and the comparison reduces to an evaluation of the properties of the used radiation source. Synchrotron radiation and γ-rays emitted by a radioactive source have very different properties. However, both types of sources permit Mössbauer experiments aiming at the extraction of hyperfine parameters, e.g., quadrupole splittings and isomer shifts. Synchrotron radiation is emitted in short (<100 ps) intense pulses that repeat periodically. On the other hand, the emission of photons from radioactive sources is random in time. The situation is inverted if we analyze the energy bandwidths, which are on the order of meV for monochromatized synchrotron radiation but only about the natural line width (Γ = 4.66 neV for the 14.4125 keV resonance of the ^{57}Fe isotope) for a suitable radioactive source. This reciprocal behavior strongly suggests that the experimental techniques should be similarly reciprocal, i.e., energy-resolved spectroscopy with radioactive sources (MBS) and time-resolved spectroscopy with synchrotron radiation (SMS). Figure 1 illustrates the spectra of a material for which the iron nuclei experience a quadrupole splitting, Δ. In conventional MBS, we observe two dips separated by Δ in the energy-dependent transmission through the material. The time-dependent transmission that is observed in SMS shows oscillations with a period of $2h/\Delta$, where h is Planck's constant. In both cases, we directly obtain the quadrupole splitting from the data. Isomer shifts are only observable in a relative sense; in the case of MBS, with respect to the source-emission line, and in the case of SMS, with respect to a reference absorber that must be inserted into the beam path.

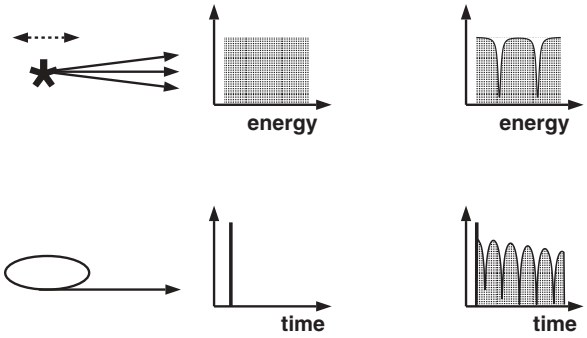

Figure 1. Reciprocal properties of radioactive sources (top) and synchrotron radiation (bottom) lead to reciprocal experimental techniques. The center panels illustrate the source characteristics averaged over a time period needed for data collection. The right panel illustrates the spectra of a material for which the iron nuclei experience a quadrupole splitting, Δ. In MBS (top), we observe two dips separated by Δ in the energy-dependent transmission through the material. The time-dependent transmission that is observed in SMS (bottom) shows oscillations with a period of $2h/\Delta$, where h is Planck's constant. In both cases, the quadrupole splitting is obtained directly from the data.

SMS experiments

Two wide-angle piston-cylinder diamond anvil cells (Mao et al. 2001) were loaded with samples of Pv05 and Pv10 for high-pressure measurements. Type-I diamond anvils with culets 300 μm in diameter (Pv10, pressures up to 75 GPa) and 100 μm in diameter (300 μm bevels) (Pv05, pressures up to 120 GPa) were used. Sample loading proceeded in the following way. First a hole of 300 μm diameter was drilled into a pre-indented disk-shaped beryllium gasket with initial dimensions of 5 mm diameter and 1 mm thickness. The hole was filled with amorphous boron, which was then pressed between two diamond anvils to a thickness of ~40 μm. Holes were drilled into the sintered boron with diameters of 100 and 50 μm for the Pv10 and Pv05 experiments, respectively. Several ruby grains were placed around the sample for pressure calibration. No pressure medium was used. After loading, the sample dimensions were $\sim 40 \times 50 \times 50\ \mu m^3$ for the Pv10 experiment and $\sim 10 \times 50 \times 50\ \mu m^3$ for the Pv05 experiment with the shortest dimension in the direction of the X-ray beam. The use of amorphous boron in this experiment is motivated by three factors: increased strength of the beryllium gasket, larger thickness of the samples and therefore higher counting rates in SMS measurements, and decreased pressure gradients across the sample. Because there was a sufficient amount of material available for Pv05, a larger sample of Pv05 was affixed to a thin plastic holder for SMS measurements under ambient conditions outside the DAC.

Experiments were performed at beamline 3-ID of the Advanced Photon Source. The X-rays were prepared with bandwidths of 2.2 meV for the measurements on Pv10 (Toellner 2000) and 1 meV for the measurements on Pv05 using multiple-crystal Bragg reflection monochromators. Due to the small sample size, focusing of the X-rays was necessary to obtain reasonable counting rates. We used a Kirkpatrick-Baez mirror system (Eng et al. 1998) to obtain a focal spot size of $6 \times 6\ \mu m^2$ at the full-width half-maximum. The X-ray flux at this spot was 10^9 ph/s (2.2 meV bandwidth) and $8 \cdot 10^8$ ph/s (1 meV bandwidth). The more efficient 1 meV monochromator is a recent development. The resulting spectral flux density

of $2 \cdot 10^{16}$ ph/s/eV/mm^2 exceeds that of common radioactive sources by more than ten orders of magnitude (Sturhahn 2004). The small X-ray spot size has the additional advantage of reducing the effects of pressure gradients on the data. The storage ring was operated in low-emittance top-up mode with 23 bunches that were separated by 153 ns. Accounting for detector-related effects, we were able to observe nuclear resonant scattering in a time window of 20 to 120 ns following excitation. Time spectra were collected on Pv05 at the following pressures: ambient, 40, 60, 85, 100, and 120 GPa. The Pv10 specimen was investigated at pressures of 3, 23, 42, 55, 65, and 75 GPa. The pressure values were determined from the R_1-fluorescence line of the ruby grains that were loaded with the samples (Mao et al. 1978), with errors of about 2 GPa at low pressures and about 5 GPa at the maximum pressure. All data were measured at ambient temperature. The data collection time per pressure point was typically two hours. The SMS spectra are shown in Figures 2 and 3.

Evaluation of SMS data

In previous MBS studies on (Mg,Fe)SiO_3 perovskite under ambient pressure conditions, the data were interpreted with several local environments and charge states of the iron atom (Jeanloz et al. 1992; Fei et al. 1994; McCammon 1997, 1998b; Lauterbach et al. 2000). Four components of the Mössbauer (MB) spectra are typically associated with iron atoms incorporated into the perovskite structure: one Fe^{3+}-like site, two Fe^{2+}-like sites, and one intermediate valence Fe^{m+} site (where $2 < m < 3$, e.g., Fei et al. 1994; McCammon 1998b; Lauterbach et al. 2000). The identification is based on the assignment of specific charge states to quadrupole splittings and isomer shifts extracted from the data. At each pressure, we started our evaluation with a simple model, with one Fe^{2+}-like site and one Fe^{3+}-like site (e.g., McCammon et al. 1992). For Pv10 at 3 and 23 GPa, this model was sufficient to explain our data. This simple model, however, cannot exclude two Fe^{2+}-like sites having very similar hyperfine parameters. For the remaining spectra, the quality of the fits were significantly improved by adding an additional Fe^{2+}-like site; that is, the data were sufficient to derive hyperfine interaction parameters of three broadened doublets that we can associate with two Fe^{2+}-like sites and one Fe^{3+}-like site (e.g., McCammon et al. 1992; Fei et al. 1994; McCammon 1997). The assumption of an additional intermediate-valence Fe site does not improve the quality of the fits. As discussed in previous works (Fei et al. 1994; McCammon 1997), two broadened Fe^{2+}-like sites in MBS data evaluation may arise from differences in the next nearest-neighbor environments. Details of the iron crystallographic-site occupancy are presented in the results and discussion section below.

As explained above and shown in Figure 1, a single doublet (quadrupole splitting and isomer shift) produces a characteristic oscillation in the time spectrum. The presence of three doublets leads to coherent superposition with respective weights and the time spectrum observed in SMS would be proportional to

$$I(t) = e^{-t/\tau} \left[w_{2,1}\cos(\omega_{2,1}t) + w_{2,2}\cos(\omega_{2,2}t) + w_3\cos(\omega_3 t)\, e^{i\delta t} \right]^2 \quad (1)$$

where w_n and $\omega_n = \pi\Delta_n/h$ are the weight and oscillation frequency, respectively, of site n (for example, $n = 2,1$ indicates Fe^{2+} site number 1). The isomer shift between the Fe^{2+} and the Fe^{3+} sites is given by δ, and $\tau = h/(2\pi\Gamma)$ is the lifetime of the nuclear excited state. This simple description does not reproduce the measured time spectra well. Perovskite samples always show a broadening of doublets in MBS spectra, which is equivalent to a distribution of quadrupole splittings (e.g., McCammon 1998b). For a Lorentzian broadening, we can give an analytic form

$$I(t) = \left[w_{2,1}\, e^{-t/\tau 2,1}\cos(\omega_{2,1}t) + w_{2,2}\, e^{-t/\tau 2,2}\cos(\omega_{2,2}t) + w_3\, e^{-t/\tau 3}\cos(\omega_3 t)\, e^{i\delta t} \right]^2 \quad (2)$$

where the distribution effects are considered by individual decay rates $\tau_n \le \tau$ (in the case of no line broadening, $\tau_n = \tau$). The full width at half maximum (FWHM) expresses this broadening (Table 1). These arguments leave us with nine adjustable parameters for each time spectrum (Table 1). For cases in which the Fe^{2+} site (n = 2,1) could be identified in the time spectrum it was not broadened, and we assumed $\tau_{2,1} = \tau$, thus reducing the number of adjustable parameters. At the highest achieved pressures, the thickness of the samples in the DAC was about 10 μm or less, which results in an effective thickness smaller than 2 (dimensionless). Effective thickness is defined as η, and $\eta = \rho\sigma f D$, where ρ is the volume density of the resonant nuclei (^{57}Fe in this case), σ is the nuclear resonant cross section, f is the Lamb-Mössbauer factor, and D is the sample thickness. Saturation of nuclear resonant absorption scales with the effective thickness, and values of less than one per resonance line, as in the present case, have negligible influence on the time spectra. For more details regarding effective thickness, the reader is referred to Sturhahn (2004) and Zhang et al. (1999). With these assumptions, the measured spectra were evaluated using the CONUSS software (Sturhahn 2000). Figure 3 displays the data and the results of the fits. Table 1 lists all the parameters from the best fits at the 90% confidence level.

Before we discuss our high-pressure results, it is prudent to assess the ambient-pressure result in light of previously performed MBS measurements on the same Pv05 material (Fei et al. 1994). Figure 2 shows a comparison of our ambient Pv05 data with a calculation (dashed line) using the ambient parameters reported in Fei et al. (1994). The inset to Figure 2 shows the corresponding energy spectra for our Pv05 ambient parameters (solid line) and those of Fei et al. (dashed line). The present data reveal different characteristics, as compared to Fei et al. (1994),

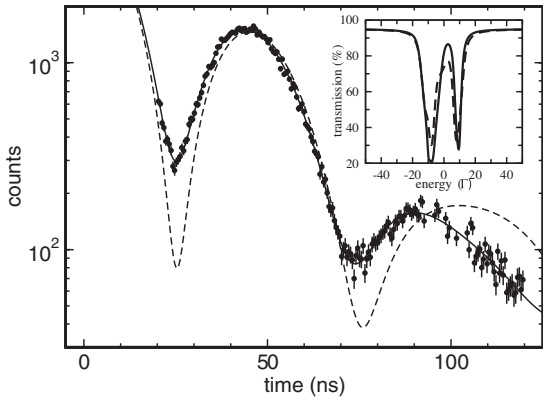

FIGURE 2. Time spectrum of Pv05 under ambient conditions (filled circles). The solid line is the calculated best-fit to our data (parameters are given in Table 1). The dashed line is obtained with the parameters given in the MBS study of Fei et al. (1994) for Pv05 at 298 K in the three-doublet model. The inset figure shows the corresponding energy spectra for our Pv05 ambient best-fit parameters (solid line) and those of Fei et al. (dashed line) in units of Γ (where Γ = 4.66 neV is the natural line width for the 14.4125 keV resonance of the ^{57}Fe isotope), calculated using CONUSS.

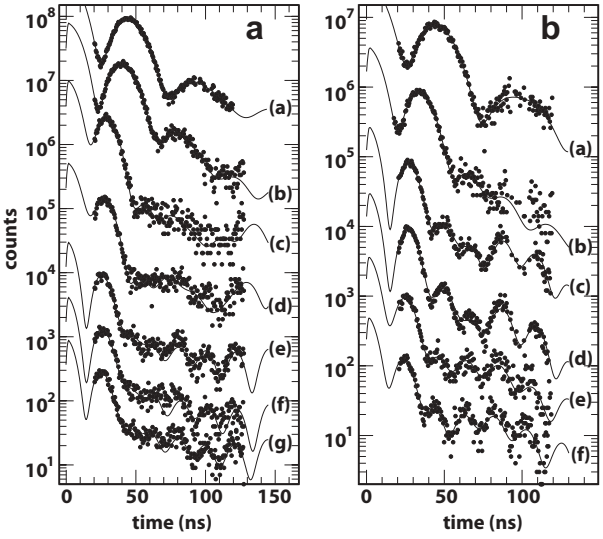

FIGURE 3. (**a**) Pv05 SMS time spectra (filled circles) and calculations with best-fit parameters given in Table 1 (solid lines) at the following pressures: (a) ambient, (b) 5 GPa, (c) 40 GPa, (d) 60 GPa, (e) 85 GPa, (f) 100 GPa, and (g) 120 GPa. The vertical axes represent intensity. (**b**) Pv10 SMS time spectra and calculations with best-fit parameters given in Table 1 at pressures of (a) 3 GPa, (b) 23 GPa, (c) 42 GPa, (d) 55 GPa, (e) 65 GPa, and (f) 75 GPa. For spectra "g" (in **a**) and "f" (in **b**) the actual collected number of events or counts are given. The other spectra are of similar statistical quality and have been offset for clarity.

TABLE 1. The best-fit parameters from the SMS time spectra evaluation

P (GPa)	Fe^{2+} 1 weight	QS (mm/s)	Fe^{2+} 2 weight	QS (mm/s)	FWHM (mm/s)	Fe^{3+} weight	QS (mm/s)	FWHM (mm/s)	IS (mm/s)
Results for $(Fe_{0.1}Mg_{0.9})SiO_3$ (Pv10)									
3	-.-	-.-	0.58	1.70(1)	0.50(7)	0.42(4)	0.68(3)	0.43(6)	–0.86(2)
23	-.-	-.-	0.60	2.20(3)	1.0(1)	0.40(7)	0.94(5)	0.57(8)	–1.11(3)
42	0.15(3)	3.37(3)	0.56	2.74(4)	0.96(6)	0.29(4)	1.51(3)	0.37(5)	–1.46(1)
55	0.13(6)	3.37(3)	0.55	2.79(3)	1.02(4)	0.32(6)	1.50(2)	0.43(4)	–1.45(1)
65	0.20(5)	3.35(6)	0.31	2.73(8)	0.35	0.48(15)	1.34(7)	0.7(1)	–1.55(5)
75	0.26(8)	3.39(7)	0.26	2.79(8)	0.28	0.48(19)	1.47(9)	0.7(2)	–1.61(6)
Results for $(Fe_{0.05}Mg_{0.95})SiO_3$ (Pv05)									
0	0.19(5)	1.89(10)	0.44	1.59(4)	0.47(3)	0.37(3)	0.57(5)	0.51(10)	–0.79(2)
5	0.10(4)	2.29(6)	0.55	1.81(5)	0.88(12)	0.35(3)	0.94(6)	0.54(9)	–0.95(2)
40	0.12(5)	3.2(2)	0.43	2.35(10)	1.1(3)	0.45(21)	1.08(12)	0.71(14)	–1.34(8)
60	0.12(8)	2.90(14)	0.31	2.59(15)	0.9(3)	0.57(28)	1.08(8)	0.67(8)	–1.38(4)
85	0.22(4)	3.49(6)	0.50	2.75(6)	1.23(16)	0.28(7)	1.65(9)	0.54(12)	–1.55(4)
100	0.22(6)	3.47(8)	0.49	2.74(7)	1.1(2)	0.29(9)	1.6(1)	0.51(15)	–1.55(5)
120	0.26(6)	3.51(6)	0.44	2.75(6)	1.1(2)	0.30(9)	1.63(10)	0.56(15)	–1.57(4)

Notes: QS – quadrupole splitting, FWHM – full width at half maximum of the QS, IS – isomer shift.
Parameters with error values were varied. The uncertainties are given in parenthesis at the 90% confidence level for the last reported significant digit(s). The weights are normalized, and therefore one of the weights is given without errors.

and are mostly due to different values for the weight of the Fe^{3+} site. Fei et al. (1994) did not report associated uncertainties with their parameters. Inspection of the bulk sample under an optical microscope reveals color heterogeneity. A possible explanation could be sample history or aging. Contrary to previous MBS experiments, the present SMS data were taken with X-rays focused to 6×6 μm^2. It is therefore expected that inhomogeneities in the sample material become noticeable. We confirmed the perovskite structure of the investigated samples by X-ray diffraction prior to each experiment, and can therefore be certain that the measured data represent the behavior of iron-bearing perovskite. Therefore, we expect our high-pressure results to reflect trends correctly. Comparisons of $Fe^{3+}/\Sigma Fe$ values obtained from previous MBS studies at ambient pressure for various iron-bearing silicate perovskite samples are listed in Table 2.

TABLE 2. Comparison with previous conventional Mössbauer measurements of iron-bearing magnesium silicate perovskite samples at ambient conditions

Reference	Cations per 3 oxygen atoms Fe	Al	$Fe^{3+}/\Sigma Fe$ (%)	capsule
This study	0.050(5)	0	37(3)	Re
Jephcoat et al. (1999)	0.05	0	9(1)	Fe
	0.06	0	16(3)	Re
Lauterbach et al. (2000)	0.092	0	16(2)	Re
	0.092	0	11(6)	Fe
	0.077	0.001	26(3)	Re
	0.106	0.001	20(3)	Fe
	0.095	0.002	27(4)	Re
McCammon (1998b)	0.05	0	9.4(1.4)	Fe
	0.06	0	16(3)	Re
McCammon (1997)	0.06	0	16(3)	Re
	0.080(7)	0.065(1)	50(5)	Re
McCammon et al. (1997)	0.06	0.03	20(6)	*
	0.08	0.20	75(3)	*
Fei et al. (1994)	0.050(5)	0	16	Re
	0.097(5)	0	20	Re
Jeanloz et al. (1992)	0.10	0	<1–3	†

Note: Citied uncertainties are given in parentheses.
* Amorphous inclusions in diamonds that have silicate perovskite compositions.
† Synthesized in a DAC at 55(5) GPa and 1700(300) K.

RESULTS AND DISCUSSION

Pressure effect on iron valence

Most relevant to geophysical models of the lower mantle is the behavior of iron in magnesium silicate perovskite, which is by far the dominant phase in Earth's lower mantle and therefore controls much of the behavior in this region. At lower mantle pressures the fraction of Fe^{3+} remains essentially unchanged. The weights from Table 1 are displayed in Figure 4 to emphasize this point. Even though we observe some variation in the weights, the data do not support a significant change in the Fe^{3+} content. This is contrary to recent suggestions that the concentration of Fe^{3+} in silicate perovskite might be sensitive to pressure (McCammon 1998b). We conclude that pressure alone (at least up 120 GPa) does not affect the valence state of iron in silicate perovskite. None of the investigated parameters indicates a charge transfer involving the Fe constituent up to 120 GPa and ambient temperature. Because several physical and chemical properties are highly dependent on the oxidation state of iron in perovskite (e.g., Mao et al. 1997; McCammon 1997), experiments under simultaneous high pressure and high temperature are imperative to further elucidate this phenomenon.

Iron site occupancy and lattice distortion

On the basis of crystal field theory (Burns 1993), spectroscopic, and X-ray diffraction measurements (e.g., Kudoh et al. 1990; Kesson et al. 1995; McCammon 1998a,b), several previous studies have demonstrated that Fe^{2+} occupies the 8–12 coordinated site in silicate perovskite. The presence of two Fe^{2+} doublets in the MB spectra, as in our case, may arise from differences in the next nearest neighbor environments in the 8–12 coordinated site, as discussed in previous works (e.g., McCammon et al. 1992; Fei et al. 1994; McCammon 1997; Lauterbach et al. 2000). The site occupancy of Fe^{3+} in silicate perovskite is less clear. Some studies suggest that Fe^{3+} may occupy the octahedral site or both cation sites in silicate perovskite according to: $^{[6]}Fe^{3+} + {}^{[8\text{-}12]}Fe^{3+} \leftrightarrow {}^{[8\text{-}12]}Mg^{2+} + {}^{[6]}Si^{4+}$ (i.e., Hirsch and Shankland 1991; McCammon et al. 1992; Fei et al. 1994; McCammon 1998a,b). In (Mg,Fe)SiO_3 perovskite, the site distribution and concentration of Fe^{3+} have been shown to be sensitive to many factors, including oxygen fugacity. Ferric iron preferentially occupies the octahedral-coordinated site under reducing conditions, whereas more oxidizing conditions and higher iron concentrations lead to broadened quadrupole doublets in MB spectra, suggesting that Fe^{3+} may substitute into both the octahedral and 8–12 coordinated sites in the perovskite structure (McCammon et al. 1992; McCammon 1998a,b). The sample used in this study was synthesized in a rhenium capsule leading to a relatively high oxygen fugacity. As in previous studies, we observed broadened

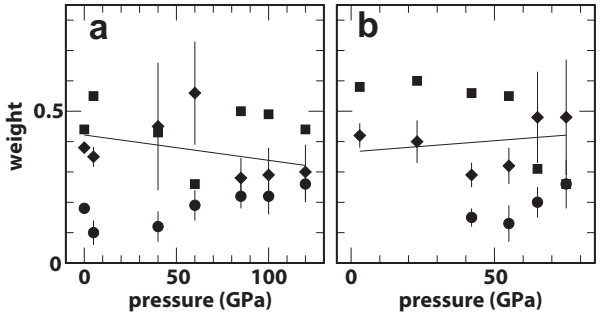

FIGURE 4. Weights of the three modeled iron sites for Pv05 (**a**) and Pv10 (**b**) as obtained from best-fits of the time spectra in Figures 3a and 3b, respectively (values are given in Table 1). In both graphs, circles and squares correspond to the Fe^{2+} 1 and Fe^{2+} 2 sites, respectively, and diamonds refer to the Fe^{3+} site. The least-squares regression lines are guides to the eye for the Fe^{3+} site.

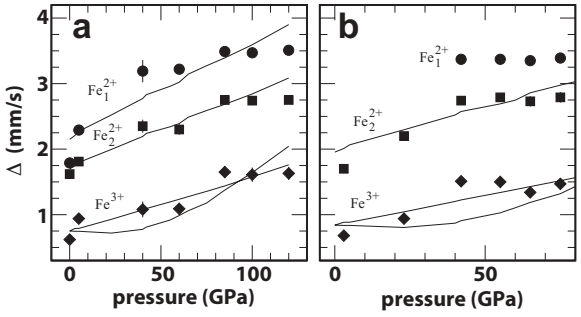

FIGURE 5. Quadrupole splittings of Pv05 (**a**) and Pv10 (**b**) derived from the time spectra (Table 1). Circles and squares correspond to the Fe^{2+} sites, diamonds to the Fe^{3+} site. The lines correspond to the electric field gradient (EFG) calculations for iron sites in Pv05 and Pv10 as a function of pressure and scaled appropriately (see text for discussion). The straight lines through the Fe^{2+} sites correspond to the EFG calculations for the Fe^{2+} behavior at the 8–12 coordinated site, scaled to the measured Fe^{2+} values. The straight and curved lines correspond to the EFG calculations for Fe^{3+} at the 8–12 coordinated and octahedrally coordinated site, respectively.

Fe^{3+} quadrupole doublets (expressed as FWHM in Table 1). In addition to previous studies, we observed the pressure dependence of the quadrupole splitting. We would like to see if the measured pressure dependence is compatible with the existing models of iron site occupancy. Our approach is to place iron ions at certain lattice sites (as described below) and calculate the expected electric field gradient (i.e., observed quadrupole splitting) under pressure-induced increasing lattice distortion.

The quadrupole splittings of all sites increase with pressure, which suggests an increasingly distorted (noncubic) local iron environment in the crystal structure (Fig. 5). We would like to understand if our observed quadrupole splitting trend is consistent with a lattice distortion effect. This explanation is corroborated with X-ray diffraction measurements on (Mg,Fe)SiO_3 perovskite to 30 GPa under hydrostatic conditions (Mao et al. 1991). These data show that (Mg,Fe)SiO_3 perovskite is elastically anisotropic, with the *b* lattice parameter being 25% less compressible than *a* and *c*. Similar results have been found in $MgSiO_3$ perovskite (Fiquet et al. 2000) and (Al,Fe)-bearing silicate perovskite (Andrault et al. 2001). The increased distortion is similarly observed from high-pressure X-ray diffraction data on the Si-O-Si tilt-angles in $MgSiO_3$ perovskite (Fiquet et al. 2000). In the Mbar range, the quadrupole splittings observed in the present study are relatively constant suggesting an increasing resistance of the lattice against further distortion. We performed electric field gradient (EFG) calculations using the point-charge model for $MgSiO_3$ perovskite with iron concentrations of 5 and 10 mol%. We assigned +2e charges to the Mg ions, +4e to the Si ions, and –2e to the O ions. The EFG calculations were carried out assuming two different scenarios that both test the iron site occupancy in silicate perovskite and assure charge neutrality of the unit cell: one scenario with an Fe ion charge of +2e at a Mg site and the other scenario with a pair of +3e charged Fe ions at neighboring Mg and Si sites. Due to the low concentrations of iron in $MgSiO_3$ perovskite, it should be possible to apply crystal field theory to these two scenarios simultaneously. The EFG was calculated as the tensor of second spatial derivatives of the Coulomb potential created by a particular arrangement of point charges:

$$V_{ab}(\mathbf{R}) = -(\partial^2 / \partial x_a \partial x_b \, \Sigma_j q_j / |\mathbf{x} - \mathbf{r}_j|)_{\mathbf{x}=\mathbf{R}}. \quad (3)$$

Here R corresponds to the position of an Fe ion, and this ion is excluded from the summation. The charges of the ions are q_j and their positions are given by r_j. The positions of the individual atoms change with compression. Even though there is no detailed information on the atomic positions, the change of the unit cell parameters has been studied by many researchers. The results of Mao et al. (1991) for (Mg,Fe)SiO_3 perovskite were used to model the pressure dependence of the atomic positions by $r_j(p) = \alpha_j a(p) + \beta_j b(p) + \gamma_j c(p)$, where the positions α, β, γ within the unit cell are assumed to be independent of pressure and a, b, and c are base vectors of the unit cell. In Figure 5, we show the largest eigenvalue of the EFG tensor (i.e., the quadrupole splitting) vs. pressure together with the results of our SMS measurements. The point-charge model usually fails to predict the quadrupole splitting value accurately because it is a simplified model and polarization effects of the atoms are neglected. By normalizing to the quadrupole splitting value of each observed site ($Fe^{2+,1}$, $Fe^{2+,2}$, and Fe^{3+}) under ambient conditions, however, we think that our calculations will still provide the right trend with increasing pressure.

In Figure 5, the pressure dependence of our EFG calculations show that the observed Fe^{2+}-like sites and Fe^{3+}-like site are consistent with their occupancy at the 8–12 coordinated site. Note that our calculated EFG trend for Fe^{2+} was applied to both the $Fe^{2+,1}$- and $Fe^{2+,2}$-like sites. Again, the two Fe^{2+}-like sites may arise from differences in next nearest-neighbor interactions at the 8–12 coordinated site. On the other hand, the noticeable distribution (expressed as the FWHM) of the observed Fe^{3+} quadrupole splitting values (Table 1), along with our EFG calculation, does not contradict the hypothesis that Fe^{3+} may occupy both cation sites, although we successfully fit our time spectra with one Fe^{3+} doublet. Based on the synthesis conditions, the observed quadrupole splitting distributions, and the EFG calculations presented here, our hypothesis that Fe^{3+} may occupy both sites is consistent with previous findings discussed above.

Pressure effect on the spin state

The observed quadrupole splittings for the Fe^{2+} sites are typical for the high-spin state of ferrous iron. The quadrupole splitting of the low-spin (or zero-spin) Fe^{2+} state would be closer to the values observed for ferric iron in the material. A zero-spin state for Fe^{2+}, for example, has been observed for octahedrally coordinated iron in (Mg,Fe)O ferropericlase above 70 GPa using XES (Badro et al. 2003). Our data show that the quadrupole splitting of Fe^{2+} remains high and that the $Fe^{3+}/\Sigma Fe$ ratio remains virtually constant at all applied pressures. On the basis of crystal-field theory (Burns 1993) and first-principles computations (Cohen et al. 1997), a zero-spin state is energetically unfavorable for Fe^{2+} at the generally assumed 8–12 coordinated site (i.e., non-octahedral) in perovskite under lower mantle pressures. We therefore infer that the divalent iron of silicate perovskite remains in a high-spin state. For Fe^{3+}, a broad distribution of quadrupole splittings (i.e., the FWHM) is observed at all pressures, and the mean quadrupole splitting value seems to be a poor indicator for the spin state of the trivalent iron component. Additional information can be gleaned from the relative isomer shift between the Fe^{3+} and Fe^{2+} sites (Fig. 6). The change in isomer shift does not depend on the lattice distortions because it results from a non-symmetry-breaking interaction. We may write for the isomer shift

$$\delta = A\,(\rho_{3+} - \rho_{2+}) \quad (4)$$

where $A < 0$ is a parameter that depends only on the resonant isotope (^{57}Fe in this case), and the symbol ρ stands for the *s*-electron densities. At lower pressures, we find that the *s*-electron density at the Fe^{3+} nuclei increases faster with pressure than at the Fe^{2+} nuclei. Figure 6 shows that the absolute value of the isomer shift increases linearly with V_0/V, i.e., with the density of the material. At $V_0/V = 1.2$, corresponding to a pressure of about 70 GPa, the relative isomer shift becomes constant. This behavior could be indicative of a change in the spin state of the Fe^{3+} ions, which influences the *s*-electron shell and thereby the isomer shift.

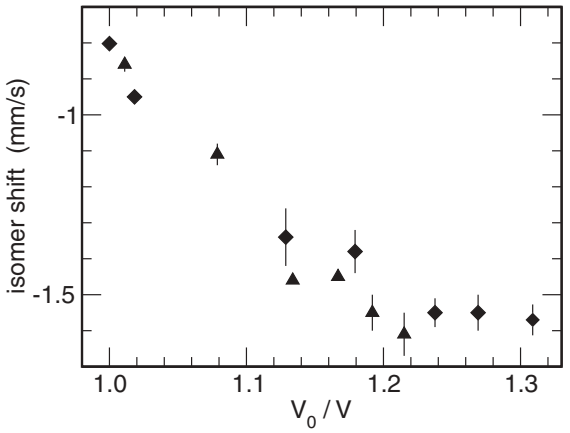

FIGURE 6. Volume dependence of the isomer shift of the Fe^{3+} site relative to the Fe^{2+} sites from fits of the time spectra for Pv10 (triangles) and Pv05 (diamonds). A change in the volume dependence of the isomer shift around $V_0/V = 1.2$ (a pressure of about 70 GPa) could be indicative of the endpoint of a continuous transition of the Fe^{3+} ions from a high-spin to a low-spin state.

To understand the role of the Fe ions in lower mantle polymorphs more completely, it is important to consider the temperature effect of such behavior. Synchrotron Mössbauer measurements on aluminous (Mg,Fe)SiO_3 perovskite, (Mg,Fe)O ferropericlase, and mixtures of these components at high pressures and temperatures would therefore lead to a more comprehensive understanding of the chemistry in the deep mantle.

ACKNOWLEDGMENTS

We thank J. Li for helpful discussions and for making the XES data available prior to publication. This manuscript benefited from comments made by D. Andrault and C. Prewitt. Support for this work was provided by the NSF and DOE under contract no. W-31-109-Eng-38 and COMPRES.

REFERENCES CITED

Alp, E.E., Sturhahn, W., and Toellner, T.S. (1995) Synchrotron Mössbauer spectroscopy of powder samples. Nuclear Instruments and Methods in Physics Research B, 97, 526–529.

Amonette, J.E., Kukkadapu, R.K., Alp, E.E., Sturhahn, W., and Toellner, T.S. (2003) Heterogeneous electron-transfer kinetics with synchrotron ^{57}Fe Mössbauer spectroscopy. Geochimica et Cosmochimica Acta, 67, 2109–2116. doi: 10.1016/S0016-7037(00)01346-7.

Anderson, D.L. and Bass, J.D (1986) Transition region of the Earth's upper mantle. Nature, 320, 321–328.

Andrault, D., Bolfan-Casanova, N., and Guignot, N. (2001) Equation of state of lower mantle (Al,Fe)-$MgSiO_3$ perovskite. Earth and Planetary Science Letters, 193, 501–508.

Badro, J., Fiquet, G., Guyot, F., Rueff, J.-P., Struzhkin, V.V., Vanko, G., and Monaco, G. (2003) Iron partitioning in Earth's mantle: Toward a deep lower mantle discontinuity. Science, 300, 789–791.

Burns, R.G. (1993) Mineralogical Applications of Crystal Field Theory. Cambridge University Press, U.K.

Cohen, R.E., Mazin, I.I., and Isaak, D.G. (1997) Magnetic collapse in transition metal oxides at high pressure: Implications for the Earth. Science, 275, 654–657.

Eng, P.J., Newille, M., Rivers, M.L., and Sutton, S.R. (1998) Dynamically figured Kirkpatrick Baez X-ray microfocusing optics. SPIE proceedings, 3449, 145.

Farges, F., Guyot, F., Andrault, D., and Wang, Y. (1994) Local structure around Fe in $Mg_{0.9}Fe_{0.1}SiO_3$ perovskite: An X-ray absorption spectroscopy study at Fe-K edge. European Journal of Mineralogy, 6, 303–312.

Fei, Y., Virgo, D., Mysen, B.O., Wang, Y., and Mao, H.K. (1994) Temperature-dependent electron delocalization in (Mg,Fe)SiO_3 perovskite. American Mineralogist, 79, 826–837.

Fiquet, G., Dewaele, A., Andrault, D., Kunz, M., and Le Bihan, T. (2000) Thermoelastic properties and crystal structure of $MgSiO_3$ perovskite at lower mantle pressure and temperature conditions. Geophysical Research Letters, 27, 21–24.

Gerdau, E. and Waard, H., Eds. (1999/2000) Nuclear resonant scattering of synchrotron radiation. Hyperfine Interactions, 123–125.

Hawthorne, F.C. (1988) Mössbauer spectroscopy. In F.C. Hawthorne, Ed., Spectroscopic methods in mineralogy and geology, 18, 255–340. Reviews in Mineralogy, Mineralogical Society of America, Washington D.C.

Hemley, R.J., Ed. (1998) Ultrahigh-pressure mineralogy, 37, 672 p. Reviews in Mineralogy, Mineralogical Society of America, Washington, D.C.

Hirose, K., Fei., Y., Ma, Y., and Mao, H.-K. (1999) The fate of subducted basaltic crust in the Earth's lower mantle. Nature, 397, 53–56.

Hirsch, L.M. and Shankland, T.J. (1991) Point defects in (Mg,Fe)SiO_3 perovskite. Geophysical Research Letters, 18, 1305–1308.

Ito, E. (1989) Stability relations of silicate perovskite under subsolidus conditions. In A. Navrotsky and D.J. Wiedner, Eds., Perovskite: A Structure of Great Interest to Geophysics and Materials Science. Geophysical Monograph 45, p. 27–32. American Geophysical Union, Washington, D.C., U.S.A.

Jackson, W.E, Knittle, E., Brown, G.E., Jr., and Jeanloz, R. (1987) Partitioning of Fe within high-pressure silicate perovskite: Evidence for unusual geochemistry in the lower mantle. Geophysical Research Letters, 14, 224–226.

Jeanloz, R. and Thompson, A.B. (1983) Phase transitions and mantle discontinuities. Reviews of Geophysics and Space Physics, 21, 51–74.

Jeanloz, R., O'Neill, B., Pasternak, M.P., Taylor, R.D., and Bohlen, S.R. (1992) Mössbauer spectrospcopy of $Mg_{0.9}Fe_{0.1}SiO_3$ perovskite. Geophysical Research Letters, 19, 2135–2138.

Jephcoat, A.P., Hriljac, J.A., McCammon, C.A., O'Neill, H.St.C., Rubie, D.C., and Finger, L.W. (1999) High-resolution X-ray powder diffraction and Rietveld structure refinement of two ($Mg_{0.95}Fe_{0.05}$)SiO_3 perovskite samples

synthesized under different oxygen fugacity conditions. American Mineralogist, 8, 214–220.
Katsura, T., Sato, K., and Ito, E. (1998) Electrical conductivity of silicate perovskite at lower-mantle conditions. Nature, 395, 493–495.
Keppler, H., McCammon, C.A., and Rubie, D.C (1994) Crystal-field charge-transfer spectra of (Mg,Fe)SiO_3 perovskite. American Mineralogist, 79, 1215–1218.
Kesson, S.E., Fitz Gerald, J.D., Shelley, J.M.G., and Whithers, R.L. (1995) Phase relations, structure and crystal chemistry of some aluminous silicate perovskites. Earth and Planetary Science Letters, 134, 187–201.
Kudoh, Y., Prewitt, C.T., Finger, L.W., Daravskikh, A., and Ito, E. (1990) Effect of iron on the crystal structure of (Mg,Fe)SiO_3 perovskite. Geophysical Research Letters, 17, 10, 1481–1484.
Lauterbach, S., McCammon, C.A., van Aken, P., Langenhorst, F., and Seifert, F. (2000) Mössbauer and ELNES spectroscopy of (Mg,Fe)(Si,Al)O_3 perovskite: a highly oxidized component of the lower mantle. Contributions to Mineralogy and Petrology, 138, 17–26.
Li, J., Struzhkin, V.V., Mao, H.-K., Shu, J., Hemley, R.J., Fei, Y., Mysen, B., Dera, P., Prakapenka, V., and Shen, G. (2003) Electronic spin state of iron in lower mantle perovskite. Eos Transaction AGU, 84, Fall Meeting Supplement, Abstract S21E-0376.
Li, X. and Jeanloz, R. (1990) Laboratory studies of the electrical conductivity of silicate perovskite at high pressures and temperatures. Journal of Geophysical Research, 95, 5067–5078.
Li, X., Ming, L.-C., Manghnani, M.H., Wang, Y., and Jeanloz, R. (1993) Pressure dependence of the electrical conductivity of $(Mg_{0.9}Fe_{0.1})SiO_3$ perovskite. Journal of Geophysical Research, 98, 501–508.
Liu, L.G. (1974) Silicate perovskite from phase transformations of pyrope-garnet at high-pressure and high-temperature. Geophysical Research Letters, 1, 277–280.
Lübbers, R., Wortmann, G., and Grünsteudel, H.F. (1999) High-pressure studies with nuclear scattering of synchrotron radiation. Hyperfine Interactions, 123/124, 529–559.
Mao, H.K., Bell, P.M., Shaner, J.W., and Steinberg, D.J (1978) Specific volume measurements of Cu, Mo, Pd, and Ag and calibration of the ruby R_1 fluorescence pressure gauge from 0.06 to 1 Mbar. Journal of Applied Physics, 49, 3276–3282.
Mao, H.K., Hemley, R.J., Fei, Y., Shu, J.F., Chen, L.C., Jephcoat, A.P., Wu, Y., and Basset, W.A. (1991) Effect of pressure, temperature, and composition on the lattice parameters and density of three (Fe,Mg)SiO_3 perovskites up to 30 GPa. Journal of Geophysical Research, 96 (B), 8069–8079.
Mao, H.-K., Shen, G., and Hemley, R.J. (1997) Multivariable dependence of Fe-Mg partitioning in the lower mantle. Science, 278, 2098–2100.
Mao, H.K., Xu, J., Struzhkin, V.V., Shu, J., Hemley, R.J., Sturhahn, W., Hu, M.Y., Alp, E.E., Vacadlo, L., Alfè, D., Price, G.D., Gillan, M.J., Schwoerer-Böhning, M., Häusermann, D., Eng, P., Shen, G., Geifers, H., Lübbers, R., and Wortman, G. (2001) Phonon density of states of iron to 153 gigapascals. Science, 292, 914–916.
McCammon, C.A. (1997) Perovskite as a possible sink for ferric iron in the lower mantle. Nature, 387, 694–696.
——— (1998a) Ferric iron in lower mantle phases. Review of High Pressure Science and Technology, 7, 52–65.
——— (1998b) The crystal chemistry of ferric iron in $Fe_{0.05}Mg_{0.95}SiO_3$ perovskite as determined by Mössbauer spectroscopy in the temperature range 80–293 K. Physics and Chemistry of Minerals, 25, 292–300.
McCammon, C., Rubie, D.C., Ross II, C.R., Seifert, F., and St.C. O'Neill, H. (1992) Mössbauer spectra of $^{57}Fe_{0.05}Mg_{0.95}SiO_3$ perovskite at 80 and 298 K. American Mineralogist, 77, 894–897.
McCammon, C.A., Hutchinson, M., and Harris, J. (1997) Ferric iron content of mineral inclusions in diamonds from São Luiz: A view into the lower mantle. Science, 278, 434–436.
McCammon, C., Peyronneau, J., and Poirier, J.-P. (1998) Low ferric iron content of (Mg,Fe)O at high pressures and temperatures. Geophysical Research Letters, 25, 1589–1592.
Miyajima, N., Fujino, K., Funamori, N., Kondo, T., and Yagi, T. (1999) Garnet-perovskite transformation under conditions of the Earth's lower mantle: an analytical transmission electron microscopy study. Physics of the Earth and Planetary Interiors, 116, 117–131.
Parise, J.B., Wang, Y., Yeganeh-Haeri, Y., Cox, D.E., and Fei, Y. (1990) Crystal structure and thermal expansion of (Mg,Fe)SiO_3 perovskite. Geophysical Research Letters, 17, 2089–2092.
Pasternak, M.P., Taylor, R.D, Jeanloz, R., Li, X., Nguyen, J.H., and McCammon, C.A. (1997) High pressure collapse of magnetism in $Fe_{0.94}O$: Mössbauer spectroscopy beyond 100 GPa. Physical Review Letters, 79, 5046–5049.
Richmond, N.C. and Brodholt, J.P. (1998) Calculated role of aluminum in incorporation of ferric iron into magnesium silicate perovskite. American Mineralogist, 83, 947–951.
Ross, N.L. and Hazen, R.M. (1990) High-pressure crystal chemistry of $MgSiO_3$ perovskite. Physics and Chemistry of Minerals, 17, 4228–4237.
Shen, G., Fei, Y., Hålenius, U., and Wang, Y. (1994) Optical absorption spectra of (Mg,Fe)SiO_3 perovskites. Physics and Chemistry of Minerals, 20, 478–482.
Sturhahn, W. (2000) CONUSS and PHOENIX: Evaluation of nuclear resonant scattering data. Hyperfine Interactions, 125, 149–172.
——— (2004) Nuclear resonant spectroscopy. Journal of Physics: Condensed Matter, 16, 5497–5530.
Sturhahn, W., Alp, E.E., Toellner, T.S., Hession, P., Hu, M., and Sutter, J. (1998) Introduction to nuclear resonant scattering with synchrotron radiation. Hyperfine Interactions, 113, 47–58.
Toellner, T.S. (2000) Monochromatization of synchrotron radiation for nuclear resonant scattering experiments. Hyperfine Interactions, 125, 3–28
Wang, Y., Guyot, F., and Liebermann, R.C. (1992) Electron microscopy of (Mg,Fe)SiO_3 perovskite: Evidence for structural phase transitions and implications for the lower mantle. Journal of Geophysical Research, 97, 12,327–12,347.
Weidner, D.J. and Wang, Y. (2000) Phase transformations: Implications for mantle structure. In S. Karato, A.M. Forte, R.C. Liebermann, G. Masters, and L. Stixrude, Eds., Earth's Deep Interior: Mineral Physics and Tomography From the Atomic to the Global Scale. Geophysical Monograph 117, 215–235. American Geophysical Union, Washington, D.C., U.S.A.
Xu, Y., McCammon, C., and Poe, B.T. (1998) The effect of alumina of the electrical conductivity of silicate perovskite. Science, 282, 922–924.
Zhang, L., Stanek, J., Hafner, S.S., Ahsbahs, H., Grünsteudel, H.F., Metge, J., and Rüffer, R. (1999) ^{57}Fe nuclear forward scattering of synchrotron radiation in hedenbergite $CaFeSi_2O_6$ at hydrostatic pressures up to 68 GPa. American Mineralogist, 84, 447–453.

MANUSCRIPT RECEIVED FEBRUARY 23, 2004
MANUSCRIPT ACCEPTED JUNE 28, 2004
MANUSCRIPT HANDLED BY ALISON PAWLEY